Engineering Failure Analysis 117 (2020) 104947

Contents lists available at ScienceDirect

Engineering Failure Analysis

journal homepage: www.elsevier.com/locate/engfailanal

Ratcheting behavior of pressurized lateral nozzle of cylinder with local wall thinning under different loading paths

Xiaohui Chen [a,*], Kaicheng Huang [a,b], Xuanchen Zhu [c], Haofeng Chen [c], Mengchao Li [a]

[a] School of Control Engineering, Northeastern University, Qinhuangdao 066004, China
[b] School of Aerospace Engineering, Xiamen University, Xiamen 361005, China
[c] Department of Mechanical & Aerospace Engineering, University of Strathclyde, G1 1XJ, UK

ARTICLE INFO

Keywords:
Lateral nozzle of cylinder
Defect
Constitutive model
Ratcheting effect
Ratcheting boundary

ABSTRACT

Ratcheting effect of pressurized lateral nozzle of cylinder with local wall thinning is studied using Chaboche model in ANSYS. Firstly, the influence of internal pressure, bending loading, loading path, loading history and the different defect sizes on ratcheting effect of pressurized oblique nozzle with local wall thinning is studied in this study. The results indicate that ratcheting strain increased with the increasing of internal pressure and bending moment and is affected by the different loading paths and loading history. Secondly, the effect of different defect sizes such as defect depth, depth length and defect hoop angle on ratcheting behavior of pressurized oblique nozzle with local wall thinning is studied. The results investigated that ratcheting strain of the lateral nozzle of cylinder with local inside wall thinning under cyclic bending increased with the increasing of defect depth, had no relationship with the increasing of defect length and ratcheting strain of the lateral nozzle of cylinder with local wall thinning under cyclic bending increased with the increasing of defect circumferential angle. Finally, the ratcheting boundary of pressurized lateral nozzle of cylinder with different defect size is determined by linear matching method. The results show that the increase of the defect depth could induce a remarkable increase of the reverse plasticity and the ratchet limits of the component, the defect length has a slight effect on the reverse plasticity and ratchet limits of the component and the increase of the defect circumferential angle could induce a remarkable increase of the reverse plasticity and the ratchet limits of the component.

1. Introduction

Pressurized pipings such as straight pipe, elbows, piping branch, lateral nozzle of cylinder and even piping systems are widely applied in nuclear, electric, and chemical industries. In addition to fluid pressure, piping components may encounter ratcheting strain under cyclic thermal stress induced from cyclic temperature or under cyclic bending initiated from seismic or the other cyclic loading such as cyclic thermal compression and extension. Ratcheting can reduce fatigue life of materials and components and seriously affect the safety and reliability of pressure vessels and piping system. Therefore, ratcheting has been considered in many design criteria for engineering components and structures, including ASME Code Section III (2007), KTA (1995), EN13445 (2002), R5 (1990) and RCC-

* Corresponding author.
E-mail address: chenxh@neuq.edu.cn (X. Chen).

https://doi.org/10.1016/j.engfailanal.2020.104947
Received 9 July 2020; Received in revised form 17 September 2020; Accepted 18 September 2020
Available online 23 September 2020
1350-6307/© 2020 Elsevier Ltd. All rights reserved.

MR (1985).

Aged pipings in the industries may have defects such as stress corrosion cracking and local thinning. Local wall thinning due to flow-accelerated corrosion was the main degradation mechanism of carbon steel piping components in nuclear power plants. Local wall thinning reduced the failure pressure, load-carrying capacity, deformation ability, and fatigue resistance of piping components. Therefore, it is important to evaluate ratcheting behavior of pressurized piping with local wall thinning in order to maintain the safety of the piping systems.

Ratcheting effect of pressurized pipe was studied by some scholars. For example, Ravi Kiran [1] presented presents methodology and a case study for seismic fragility analysis of pressurized piping systems considering ratcheting. Seismic fragility curves are generated for a typical stainless steel piping system which was considered for OECD-NEA benchmark exercise on seismic margin assessment. Karimi [2] investigated ratcheting behavior of SS316 L thin-walled steel pipes subjected to cyclic internal pressure experimentally and numerically. The results showed that the ratcheting strain was only significant in the hoop direction of a pipe subjected to cyclic internal pressure. The results indicated that the experimental and numerical results were in good agreement. Bao [3] studied ratcheting tests of Z2CND18.12N austenitic stainless steel elbow pipes under reversed in-plane load of 20 kN and constant pressure of 17.5 MPa after thermal aged 1000 h and 2000 h respectively at the same thermal aging temperature of 500 centigrade degrees. The results indicate that the ratcheting behavior of pressurized elbow pipe is prominently affected by thermal aging. Simulation results are perfectly agreement with experimental data. Ratcheting shakedown boundaries of thermal aged elbow pipes were determined by CJK model. Hassan and his collaborators [4,5] studied respectively ratcheting strain of alloy steel 4130 straight pipe and stainless steel (SS) 304L elbow at room temperature, and low-cycle fatigue and ratcheting responses of SS 304L 90° short and long radius elbows at room temperature and high temperature subjected to repeated reversal force or displacement loading through experimental and analytical methods. Zakavi and his collaborators [6–8] observed that ratcheting behavior of carbon steel and stainless steel cylindrical specimens pressurized cylinders subjected to dynamic bending moment or seismic loading. Varelis and his collaborators [9,10] investigated the low-cycle fatigue of pipe elbows by means of experiments and determined an accurate numerical model for pipe elbows under severe cyclic in-plane bending, simulating earthquake level loading. Based on the previous experimental work, the numerical models for steel elbow elastic–plastic behavior under cyclic in-plane bending were developed.

Chen et al. [11] presented an overview of recent progresses in experimental investigation and finite element analysis (FEA) of ratcheting behavior of pressurized piping. Based on experimental and FEA research, ratcheting boundaries have been determined with the final aim of aiding the safety design and assessment of engineering piping structures. The number of experiments on the ratcheting behavior of pressurized pipes was limited because these experiments were expensive, laborious, and time consuming. It was preferable to establish finite element method to simulate the experimental procedure. On the basis of experiments and finite element analysis, Chen and his team [12–17] studied multiaxial ratcheting for pressurized low carbon steel and austenitic stainless steel Z2CND18.12N straight pipe and elbows with and without local wall thinning under reversed bending. The maximum ratcheting strain of pressurized elbow occurred mainly in the circumferential direction at flanks.

In order to prevent ratcheting effect, it is necessary that ratcheting boundary is determined by the ratcheting criteria in standard code or the proposed simple method. The ratcheting effect has been considered in several standards, such as ASME (2017), KTA (2014) and RCC-MR (2007). Ratcheting boundary was studied by several scholars. Chen et al. [12,13] employed elastic–plastic finite element analysis combined with the Committee of Three Dimensional Finite Element Stress Evaluation (C-TDF) in Japan which determined ratcheting boundary of straight pipe and elbow. Shen et al. [18] proposed a new four-dimensional ratcheting boundary for the first time considering the interaction among four types of stresses: constant mechanical membrane stress and mechanical bending stress, cyclic thermal membrane stress and thermal bending stress. On the basis of Tresca yield condition and elastic-perfectly plastic behavior, a novel two-plane FE model was built for numerical validation and results predicted by analytical solution agreed very well with that obtained by two-plane FE model. The relationship of the three-dimensional ratcheting boundary adopted by the newly implemented ASME VIII-2 Pressure Vessel Code and this four-dimensional ratcheting boundary considering constant mechanical membrane stress and mechanical bending stress, cyclic thermal membrane stress and thermal bending stress simultaneously was also discussed. Adibi-Asl and Reihardt [19] proposed a non-cyclic method for assessing the shakedown- ratchet boundary based on a lower bound formulation by decomposing the loading into mean (time-invariant) and fully reversed proportional components. The fundamental idea behind the proposed method was to (conservatively) determine the ratchet boundary without going through the cyclic history. In this approach the shakedown analysis was reduced to limit analysis by considering the contribution of cyclic load components. According to the non-cyclic method, Zheng et al. [20] deduced theoretically ratchet limits of cylindrical pipelines subjected to several typical cyclic non-proportional loading combinations, such as internal pressure, tension, compression, moment, torsion, and thermal loading in practical engineering. Chen et al. [21] proposed a computational process for identifying the shakedown-ratchet boundary based on an extension of the classical upper bound shakedown theorem. Since the method is constructed based on an upper bound formulation, full convergence of the solution is required to obtain a design estimate of the ratchet boundary.

In the present study, firstly, the ratcheting behavior for a lateral nozzle of cylinder with local wall thinning under reversed bending is studied using finite element method, considering the influence of internal pressure, bending loading, loading paths and loading history on ratcheting effect. Secondly, the effect of defect size on ratcheting strain of the lateral nozzle of cylinder with local wall thinning is studied. Finally, ratcheting boundary of the lateral nozzle of cylinder with local wall thinning is determined by linear matching method.

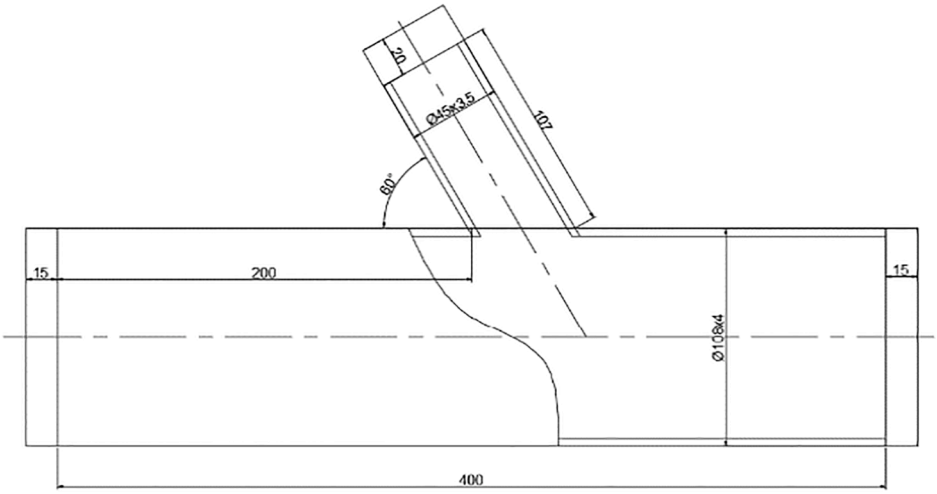

(a) Geometry model

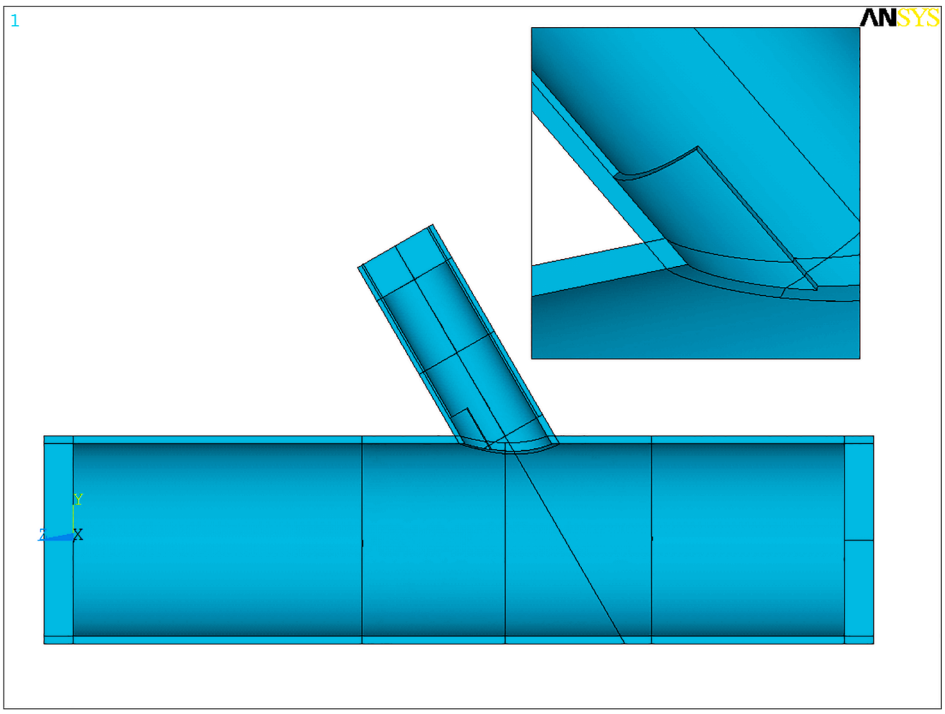

(b) Finite element model

Fig. 1. Pressured oblique nozzle model.

Table 1
Main geometrical parameters of pressured geometry.

Component	Parameters	Value
Straight tube	Diameter *Ds* (mm)	108
	Thickness *Ts* (mm)	4
Oblique nozzle	Angle (°)	60
	Diameter *Do* (mm)	45
	Thickness *To* (mm)	3.5

Table 2
Dimensionless parameters of defect.

No.	Defect depth proportion: d/t	Defect length proportion: θ/π	Defect angle proportion: h/L
1	0.3	10%	1/6
2	0.5	20%	1/3
3	0.7	30%	1/2

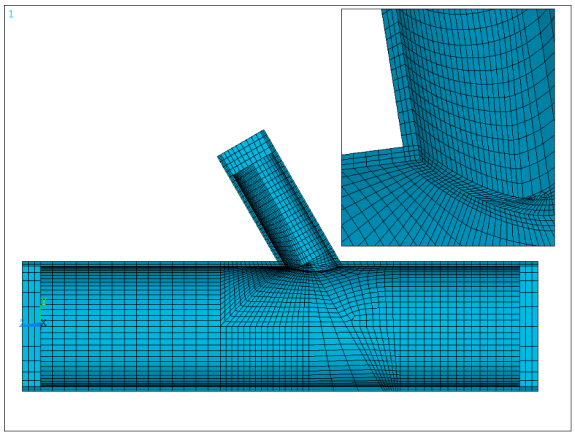

Fig. 2. Finite element model of pressured pipeline.

2. Finite element model

2.1. Geometrical model and mesh arrangement

Yang [22] studied ratcheting effect of the oblique nozzle by the experiments and finite element analysis as shown in Fig. 1(a). The main geometrical parameters are given in the Table 1. The shape of local wall thinning is rectangle which contains three sizes such as defect depth, depth length and defect hoop angle. Xia [23] proposed dimentionless semiellipsoid thinning parameters, including depth proportion, circumferential angle proportion and height proportion shown in Table 2. And Liu [24] simplified the thinning as rectangle. Therefore, this study tried to simplify the thinning as circumferential rectangle, which lied in the acute joint part of the oblique nozzle. Choose the depth proportion is 0.3, circumferential angle proportion is 1/6 and the height proportion is 10%. Therefore, the defect depth is 1.05 mm, depth length 9.4 mm and depth hoop angle 30° angle, shown as Fig. 1(b).

Three dimensional isoparametric element solid 95 which is used in this study. It is a higher-order version of solid 45 and has a great tolerance of irregular shapes. It is used to generate the finite element method mesh of the cylinder with nozzle. Considering the symmetry of the model, 1/2 model would be established by ANSYS, as given in Fig. 1. Three elements are modeled throughout the thickness. Fig. 2 indicates the mesh for the cylinder with nozzle. The total number of elements is 12547. The intersection of the cylinder and nozzle has a very fine mesh with large number of elements. The accuracy of results is also studied by means of double meshes [25]. Comparison of the twice results of finite element analysis, the error of both results was 3–5%. The results indicated that the first element number is suitable.

The boundary conditions used in the finite element numerical simulation are set as follows: all nodes on the symmetric section (longitudinal plane of the vessel) are constrained against deformation in the direction normal to the symmetric plane. The node located at the center of one saddle support is restricted in the vertical direction only. The internal pressure loading of the analysis model is loaded incrementally inside the surface of the cylinder and nozzle.

Table 3
The Chaboche model parameters.

σ_x (MPa)	E (MPa)	γ_1	γ_2	γ_3	C_1 (MPa)	C_2 (MPa)	C_3 (MPa)
100	2.1×10^5	2×10^4	10^3	3	2.5×10^6	9.43×10^4	4×10^3

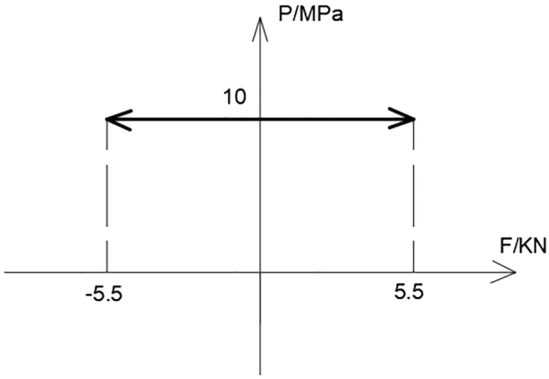

Fig. 3. Path of bending moment and internal pressure.

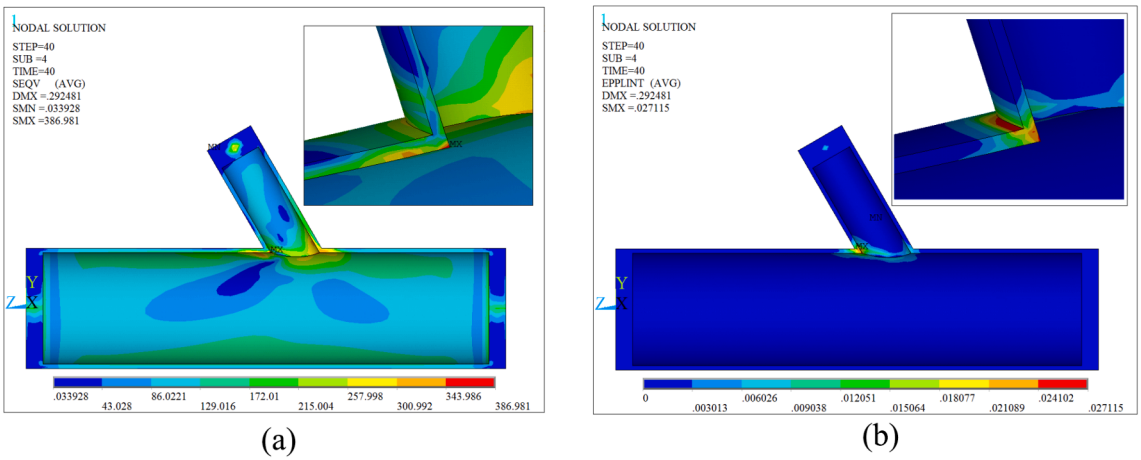

(a) (b)

Fig. 4. Von Mises stress and plastic strain contour of lateral nozzle of cylinder.

2.2. Chaboche model and constitutive parameters

Chaboche [26] modified the classical Armstrong-Frederic (A-F) kinematic hardening material law by superimposing two classical A-F hardening laws and a special law [27]. It can be combined with any available isotropic hardening models and useful in analyzing objective cyclic plastic behavior, including the model's ratcheting behavior. The model is shown as:

$$\boldsymbol{\alpha} = \sum_{i=1}^{M} \boldsymbol{\alpha}_i, \quad d\boldsymbol{\alpha}_i = \frac{2}{3} C_i d\boldsymbol{\varepsilon}_p - \gamma_i \boldsymbol{\alpha}_i dp \quad \text{for } i = 1, 2, 3 \tag{1}$$

$$\sum_{i=1}^{M} \boldsymbol{\alpha}_i + \sigma_0 = \sigma_x \tag{2}$$

$$\boldsymbol{\alpha}_i = \frac{C_i}{\gamma_i}\left[1 - exp\left(\gamma_i \varepsilon_x^p\right)\right] \tag{3}$$

$$\frac{C_1}{\gamma_1} + \frac{C_2}{\gamma_2} + \sigma_0 = \sigma_x - \frac{C_3}{2}\left\{\varepsilon_x^p - \left(-\varepsilon_L^p\right)\right\} \tag{4}$$

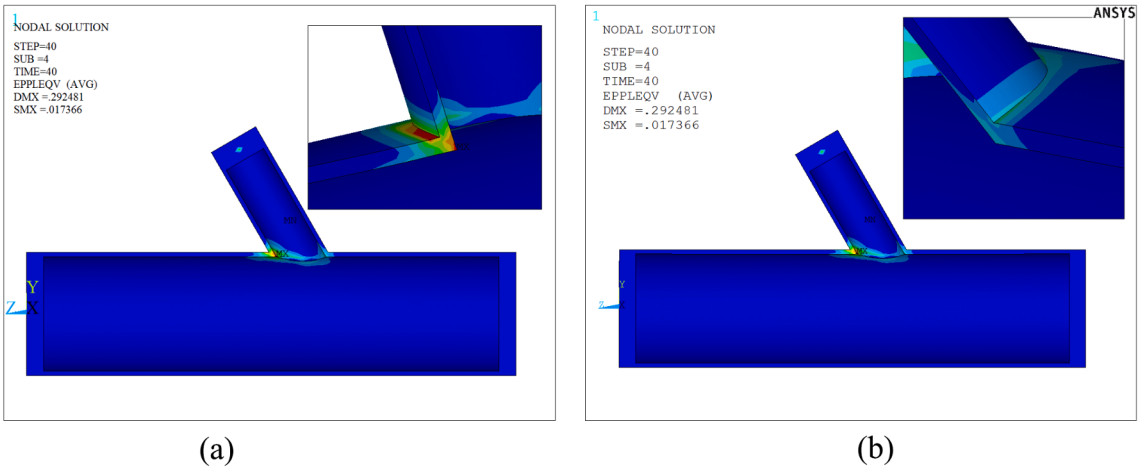

(a) (b)

Fig. 5. Von Mises plastic strain contour of lateral nozzle of cylinder without local wall thinning.

The Chaboche model parameters are shown in Table 3 after calculating [19].

2.3. Ratcheting behavior of pressured lateral nozzle of cylinder under cyclic bending loading

Fig. 3 gave ratcheting behavior of lateral nozzle of cylinder with and without local wall thinning subjected to internal pressure of 10 MPa and cyclic loading of $\Delta F/2 = 11$ kN, namely loading path. Constant internal pressure of 10 MPa was applied to inner surface of the lateral nozzle of cylinder and the bending load of $\Delta F/2 = 11$ kN was applied to Y direction of the pipe block center of oblique nozzle. Fig. 4 showed von Mises stress contour and plastic strain contour of 20 cycles. The maximum von Mises stress and plastic strain occurs in the interaction region of the cylinder and oblique nozzle with and without local wall thinning. Point A and Point B in Fig. 5 will be studied in the following.

The stress – strain relationships of the Point A and Point B of lateral nozzle of cylinder with and without local wall thinning is shown in Fig. 6. It is found that plastic strain accumulates with the increasing of the number of cycles. Accumulation plastic strain of Point A is larger than that of Point B. Accumulation plastic strain of lateral nozzle of cylinder with local wall thinning is larger than that of lateral nozzle of cylinder without local wall thinning.

The ratcheting strain of the Point A and Point B of lateral nozzle of cylinder with and without local wall thinning is compared, as shown in Figs. 7 and 8. On the basis of the strain history in each direction, ratcheting strain, namely first principal strain, which is determined according to the midpoint method. Under the same internal pressure and cyclic loading, ratcheting strain at Point A of lateral nozzle of cylinder with local wall thinning in Fig. 8 is larger than that of lateral nozzle of cylinder without local wall thinning; ratcheting strain at Point B of lateral nozzle of cylinder with local wall thinning is smaller than that of lateral nozzle of cylinder without local wall thinning.

The hoop and axial ratcheting strain of the Point A of lateral nozzle of cylinder with and without local wall thinning subjected to the same loading is compared, as given in Fig. 9. It indicates that hoop and axial ratcheting strain at Point A of lateral nozzle of cylinder with local wall thinning is larger than that of lateral nozzle of cylinder without local wall thinning. Ratcheting strain occurs mainly circumferential direction of the lateral nozzle of cylinder.

3. Ratcheting strain of pressured lateral nozzle of cylinder with local wall thinning

3.1. Effect of internal pressure on ratcheting behavior

The influence of internal pressure on ratcheting strain of lateral nozzle of cylinder with local wall thinning is given in Fig. 9. Constant internal pressure of 10 MPa, 20 MPa and 30 MPa was applied to inner surface of lateral nozzle of cylinder with local wall thinning, respectively. The bending load of −5.5 kN to 5.5 kN ($\Delta F/2 = 11$ kN) was applied to y direction of the pipe block center of oblique nozzle. It is found from Fig. 9 that ratcheting strain increases with the increasing of internal pressure. Fig. 9(b) indicates that hoop ratcheting strain of lateral nozzle of cylinder with local wall thinning is larger than axial ratcheting strain.

3.2. Effect of bending loading on ratcheting behavior

Fig. 10 shows the influence of cyclic bending loading on ratcheting strain of lateral nozzle of cylinder with local wall thinning. The bending load of $\Delta F/2 = 11$ kN, $\Delta F/2 = 15$ kN and $\Delta F/2 = 19$ kN was applied to Y direction of the pipe block center of oblique nozzle, respectively. Constant internal pressure of 10 MPa is applied to inner surface of lateral nozzle of cylinder with local wall thinning, respectively. Fig. 11 investigates that ratcheting strain increases with the increasing of internal pressure. It is shown in Fig. 10(b)

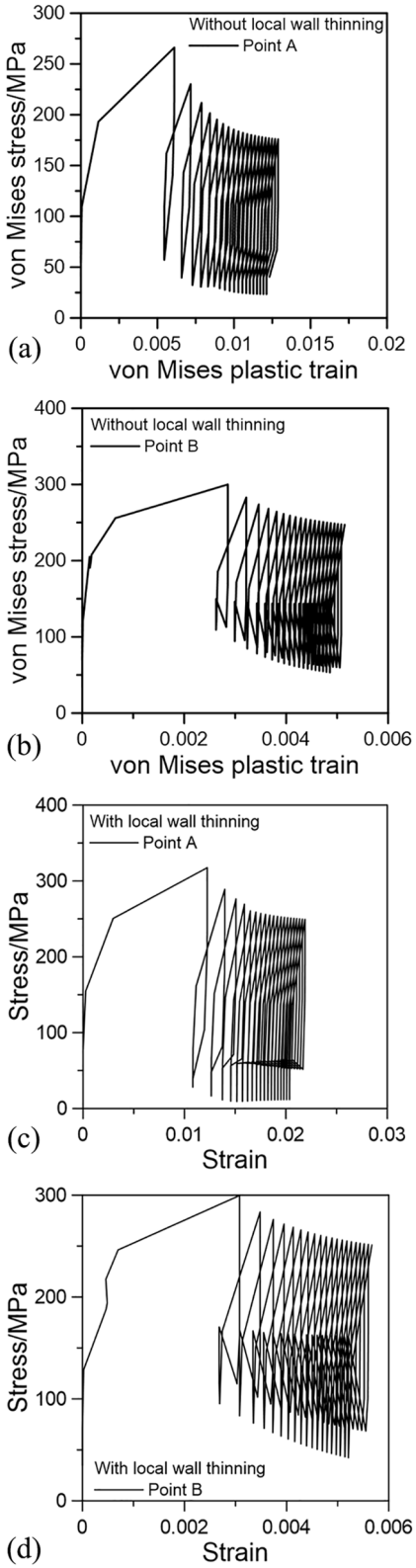

Fig. 6. Strain-stress relationships of the Point A and Point B.

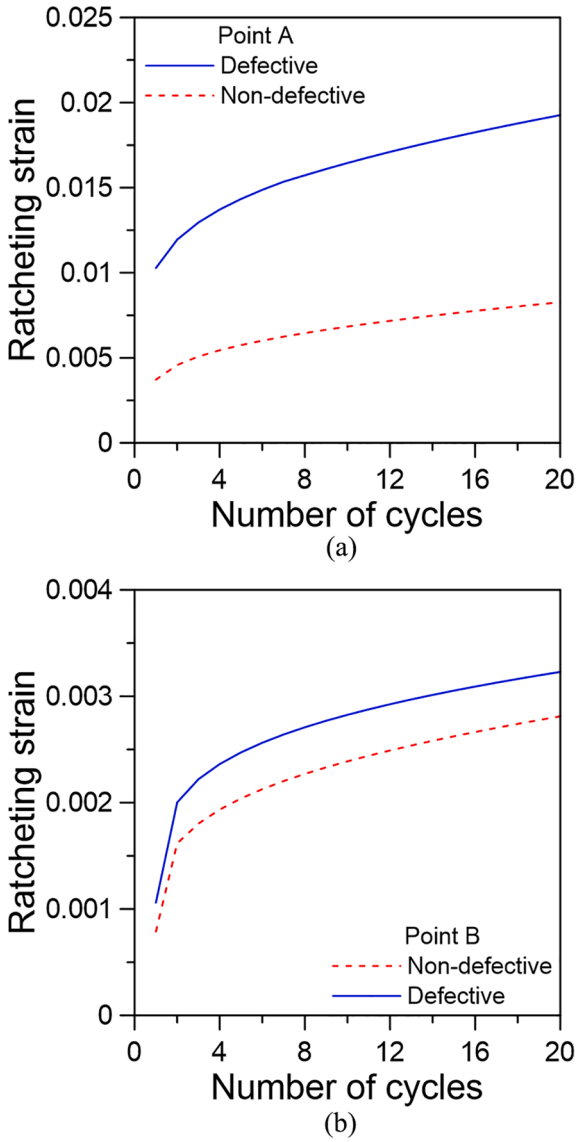

Fig. 7. The ratcheting strain prediction curve of pressured pipelines.

indicates that hoop ratcheting strain of lateral nozzle of cylinder with local wall thinning is larger than axial ratcheting strain.

3.3. Effect of loading paths on ratcheting behavior

The pipeline often works the changing environment, the different environmental factors would change its loading conditions. Therefore, it is significant to study its strain response under alternating loading of internal pressure and bending moment, as shown in Fig. 11. The simulated paths are shown in Fig. 11. For paths 1 and 3, the internal pressure is constant when bending moment change from tensile to compression, the alternating process of internal pressure and bending moment evolved along with counterclockwise direction.

Path 1 is a rectangle path evolved along with counterclockwise direction. A single cycle includes four loading steps. Path 2 is a right triangle path evolved along with counterclockwise direction. A single cycle includes three loading steps. Path 3 is an isosceles triangle path evolved along with counterclockwise direction. A single cycle includes three loading steps. Path 4 is symmetrical with path 2, which also evolved along with counterclockwise direction. A single cycle includes three loading steps.

The ratcheting strain prediction curve of the Point A of defective model would be shown as Fig. 12 by ANSYS 19.2 software. It investigated that ratcheting strains of the lateral nozzle of cylinder with local wall thinning under loading path 2 and loading path 3 were almost identical. The ratcheting strain of the lateral nozzle of cylinder with local wall thinning under loading path 4 was minimum.

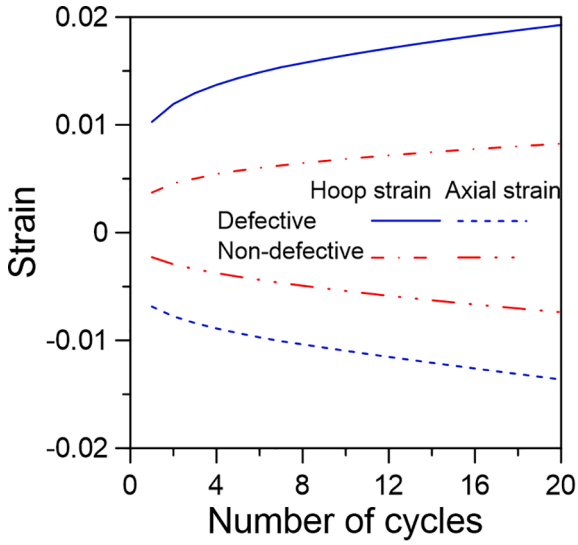

Fig. 8. The hoop strain and axial strain curve of pressured pipeline.

3.4. Effect of loading history on ratcheting behavior

Fig. 13 gives ratcheting strain with loading history 1 of the lateral nozzle of cylinder with local wall thinning subjected to 10 MPa of internal pressure and 11 kN, 15 kN and 19 kN of in plane opening bending loads. It reveals that the ratcheting strain rate increases with a bending load under the same internal pressure.

Ratcheting strain with loading history 2 of the lateral nozzle of cylinder with local wall thinning subjected to 10 MPa of internal pressure and 19 kN, 15 kN and 11 kN of in plane opening bending loads is given in Fig. 14. It also observes that the ratcheting strain rate increases with a bending load under the same internal pressure.

As the above shown, when the number of cycles is between 21 and 40, the predicted results under loading history 1 is higher than loading history 2 obviously, the slope under loading history 1 is more than that loading history 2. And it's obvious that the cyclic progressive loading history have more obvious influence than the cyclic reduced loading history. So we can conclude that the loading history has great influence to the pipeline ratcheting effect and the ratcheting strain curve would slow down after the larger bending moment action.

4. The effect of local wall thinning on ratcheting strain of lateral nozzle of cylinder with local wall thinning

The influence of depth, length and circumferential angle of local wall thinning at the nozzle on the ratcheting behavior of pressurized lateral nozzle of cylinder subjected to reversed in-plane bending was also studied in the study. The geometric dimensioning of local wall thinning was listed in Table 4.

In the following, all the lateral nozzle of cylinders with different local wall thinning were subjected to constant internal pressure of 10 MPa and the cyclic bending load of $\Delta F/2 = 11$ kN.

4.1. Effect of defect depth on ratcheting behavior

The effect of different depth of local wall thinning on ratcheting strain of the lateral nozzle of cylinder is given in Fig. 14. The dimension with defect length of 9.4 mm and circumferential angle of 30° of local wall thinning is kept constant. The defect depth is 1.05 mm, 1.75 mm and 2.45 mm respectively. Ratcheting strain of the lateral nozzle of cylinder with local inside wall thinning under cyclic bending increases with the increasing of defect depth. Fig. 14(b) observes that hoop ratcheting strain of lateral nozzle of cylinder with local wall thinning is almost the same as axial ratcheting strain.

4.2. Effect of defect length on ratcheting behavior

Fig. 15 shows the influence of different length of local wall thinning on ratcheting strain of the lateral nozzle of cylinder. The defect length is 9.4 mm, 18.8 mm and 28.2 mm respectively. The dimension with defect depth of 1.05 mm and circumferential angle of 30° of local wall thinning is kept constant. Ratcheting strain of the lateral nozzle of cylinder with local wall thinning under cyclic bending had no relationship with the increasing of defect length. Fig. 15(b) indicates that axial and hoop ratcheting strain of lateral nozzle of cylinder with local wall thinning is almost the same.

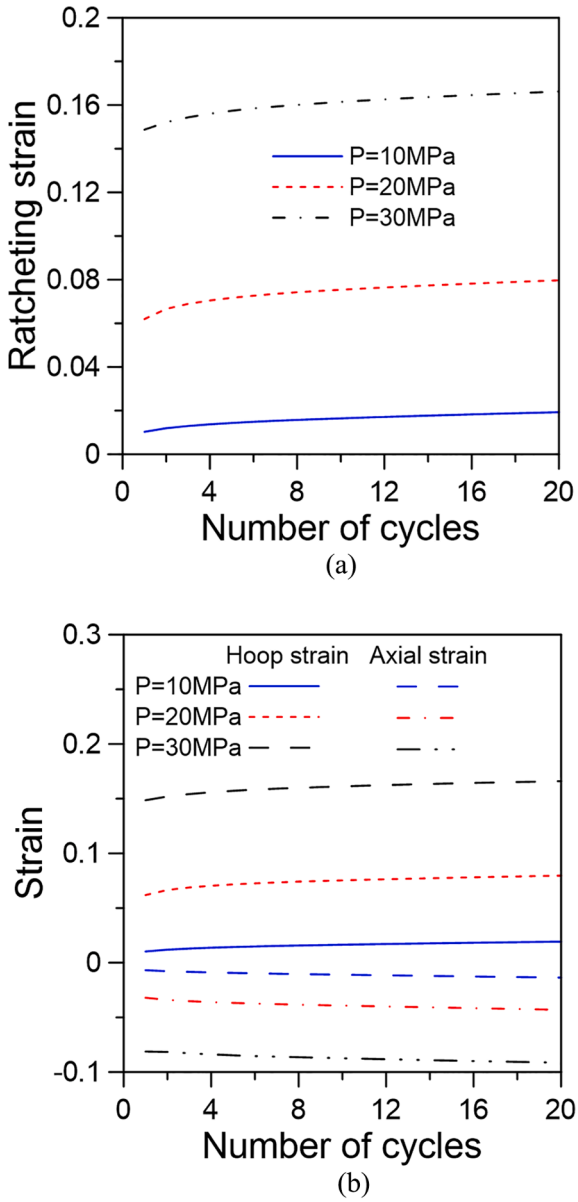

Fig. 9. Ratcheting strain of the Point A.

4.3. *Effect of defect circumferential angle on ratcheting behavior*

The influence of different defect circumferential angle of local wall thinning on ratcheting strain of the lateral nozzle of cylinder is shown in Fig. 16. The defect circumferential angle is 30°, 60° and 90° respectively. The dimension with defect length of 9.4 mm and defect depth of 1.05 mm of local wall thinning is kept constant. It was seen in Fig. 16 that ratcheting strain of the lateral nozzle of cylinder with local wall thinning under cyclic bending increases with the increasing of defect circumferential angle. Fig. 16(b) observes that ratcheting strain of lateral nozzle of cylinder with local wall thinning occurred in the circumferential and meridional directions.

5. Ratcheting boundary

5.1. C-TDf

The C-TDF [28,29] in Japan proposed one criteria to verify shakedown. The content of the criteria was that ''Variations in equivalent plastic strain at the end of each cycle should have a deceasing trend and should become lower than the allowable limit of 10^{-4}/cycle''. Five or ten cycles were required to achieve this value. In this paper, ten cycles are used to determine ratcheting boundary

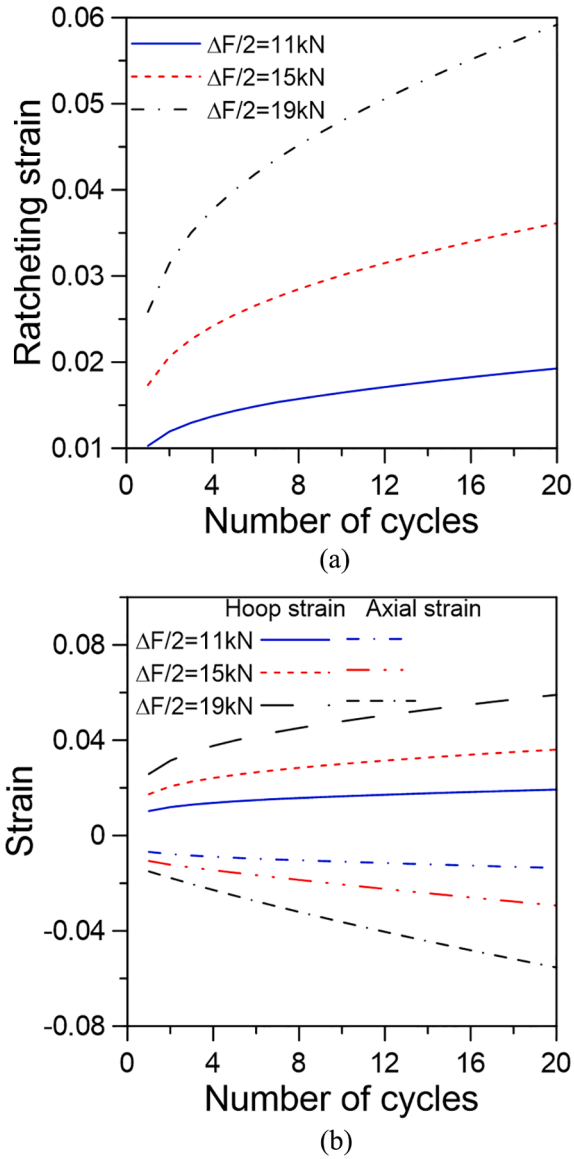

Fig. 10. Ratcheting strain of Point A.

of the pipes.

5.2. Linear matching method (LMM)

Chen and Ponter [21] described in detail LMM framework for ratchet analysis. The material is regarded as isotropic, elastic-perfectly plastic and satisfies the von Mises yield conditions. A typical cycle in the time interval $0 \leqslant t \leqslant \Delta t$ is considered. Considering the cyclic problem, an elastic plastic body is subjected to a cyclic history of varying temperature $\lambda_\theta \theta(x,t)$ within the volume of the structure and varying surface loads $\lambda_P P(x,t)$ which act over part of the structure's surface S_T, where, λ denotes a load parameter, allowing a whole class of loading histories to be taken into account. On the remainder of the surface S, denoted as S_u, the displacement $u = 0$. The corresponding linear-elastic solution history of loading histories is shown as

$$\lambda \widehat{\sigma}_{ij}(x,t) = \lambda_p \widehat{\sigma}^p_{ij}(x,t) + \lambda_\theta \widehat{\sigma}^\theta_{ij}(x,t) \tag{5}$$

where $\widehat{\sigma}^p_{ij}(x,t)$ and $\widehat{\sigma}^\theta_{ij}(x,t)$ are the linear elastic solutions corresponding to varying surface $P(x,t)$ and temperature $\theta(x,t)$, respectively.

For the cyclic problem, the stresses and strain rates will become asymptotic to a cyclic state where;

$$\sigma_{ij}(t) = \sigma_{ij}(t+\Delta t), \quad \dot{\varepsilon}_{ij}(t) = \dot{\varepsilon}_{ij}(t+\Delta t) \tag{6}$$

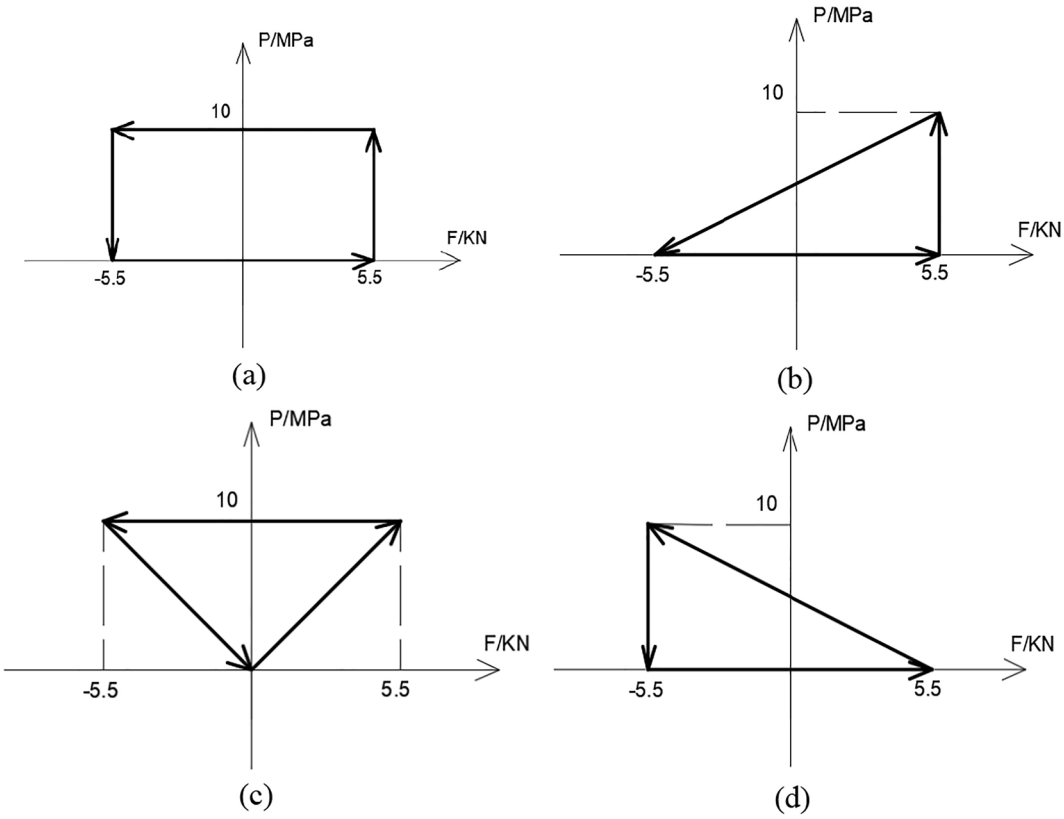

Fig. 11. Paths of alternation of bending moment and internal pressure.

The cyclic solution is composed of three parts, the elastic solution, a transient solution accumulated up to the beginning of the cycle and a residual solution that on behalf of the remaining changes within the cycle. The cyclic stress history irrespective of material properties is given by

$$\sigma_{ij}(x,t) = \lambda\widehat{\sigma}_{ij}(x,t) + \overline{\rho}_{ij}(x) + \rho^{r}_{ij}(x,t) \tag{7}$$

where $\overline{\rho}_{ij}(\boldsymbol{x})$ denotes a constant residual stress field in equilibrium with zero surface traction on S_T and corresponds to the residual state of stress at the beginning and end of the cycle. The history $\rho^{r}_{ij}(\boldsymbol{x},t)$ is the change in residual stress during the cycle which satisfies

$$\rho^{r}_{ij}(x,0) = \rho^{r}_{ij}(x,\Delta t) \tag{8}$$

For ratchet analysis, an incremental minimization can give the history of the varying residual stress field corresponding to the cyclic part of the load history. Then, Ref. [21] has proved that the numerical procedure of ratchet analysis can be adapted to the existing procedure of shakedown analysis where the linear elastic solution is replaced by the calculated varying residual stress field, i.e.

$$\widehat{\sigma}_{ij}(x,t) = \lambda\widehat{\sigma}_{ij}^{\overline{C}} + \widehat{\sigma}^{\Delta}_{ij}(x,t) + \rho_{ij}(x,t) \tag{9}$$

Combining the von Mises yield condition and corresponding flow rule, an upper bound of ratchet limit is then calculated by

$$\lambda = \frac{\int_V \sum_{n=1}^{N} \sigma_y \overline{\varepsilon}\left(\Delta\varepsilon^{n}_{ij}\right)dV - \int_V \sum_{n=1}^{N}\left(\widehat{\sigma}^{\Delta}_{ij}(t_n) + \rho_{ij}(t_n)\right)\Delta\varepsilon^{n}_{ij}dV}{\int_V \widehat{\sigma}_{ij}^{\overline{C}}\left(\sum_{n=1}^{N}\Delta\varepsilon^{n}_{ij}\right)dV} \tag{10}$$

Eq. (10) provides the method to calculate the capacity of the structure subjected to a predefined cyclic load to bear an additional constant load before ratchet behavior happens.

As described in Melan's lower bound theorem, once the changing residual stress field $\rho^{r}_{ij}(\boldsymbol{x},t)$ and the constant residual stress $\overline{\rho}_{ij}(\boldsymbol{x})$ in Eq. (7) have been calculated by global minimization and incremental minimization, we can construct the calculating of the lower bound of shakedown or ratchet limit within the upper bound procedure through maximizing the lower bound load parameter λ_{LB} if any potential stable cyclic stress caused by corresponding active loading history within the limit of yielding.

Because of a sequence of upper bound iterative process give the residual stress field, we can then scale the elastic solution to calculate the lower bound at each iteration so that the stable cyclic stress nowhere violate the yield condition. The lower bound of

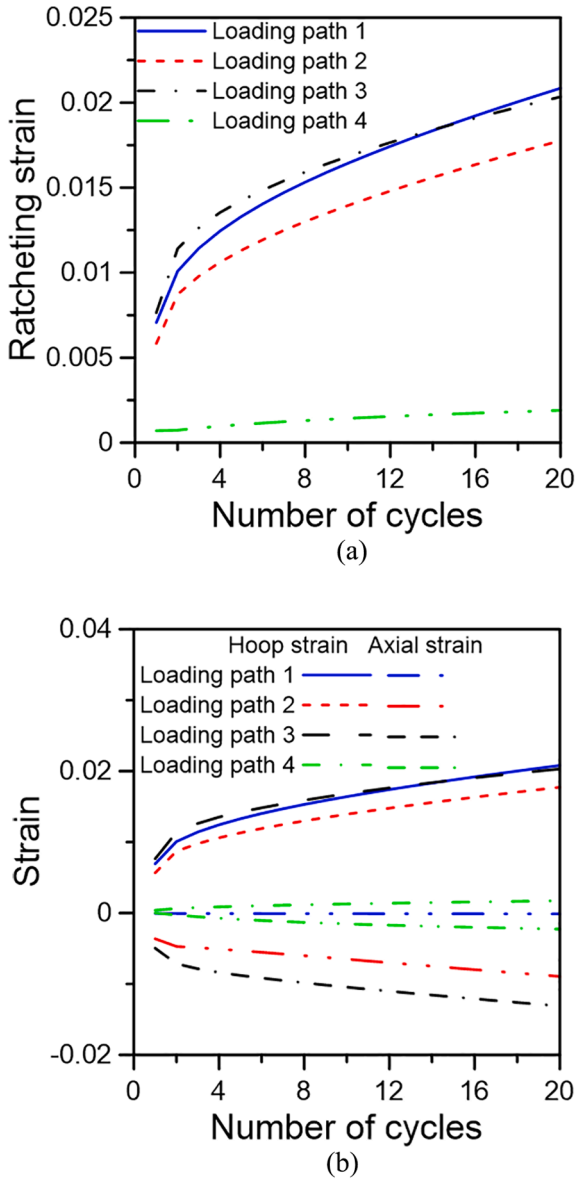

Fig. 12. The ratcheting strain prediction curve of the Point A of defective model.

shakedown limit multiplier is calculated by

$$\lambda_{LB}^{s} = max\lambda_{LB} \tag{11a}$$

$$s.t. \quad f\left(\lambda_{LB}\widehat{\sigma}_{ij}(x,t) + \overline{\rho}_{ij}(x)\right) \leqslant 0 \tag{11b}$$

The lower bound of ratchet limit multiplier is given by

$$\lambda_{LB}^{R} = max\lambda_{LB} \tag{12a}$$

$$s.t. \quad f\left(\lambda_{LB}\widehat{\sigma}_{ij}^{F} + \widehat{\sigma}_{ij}^{\Delta}(x,t) + \rho_{ij}(x,t) + \overline{\rho}_{ij}(x)\right) \leqslant 0 \tag{12b}$$

The LMM is based on elastic-perfectly plastic material, thus, the material properties for the LMM model contains elastic modulus $E = 1.9 \times 10^5$ MPa, Poisson's ratio $\upsilon = 0.3$, yield stress $\sigma_y = 320$ MPa.

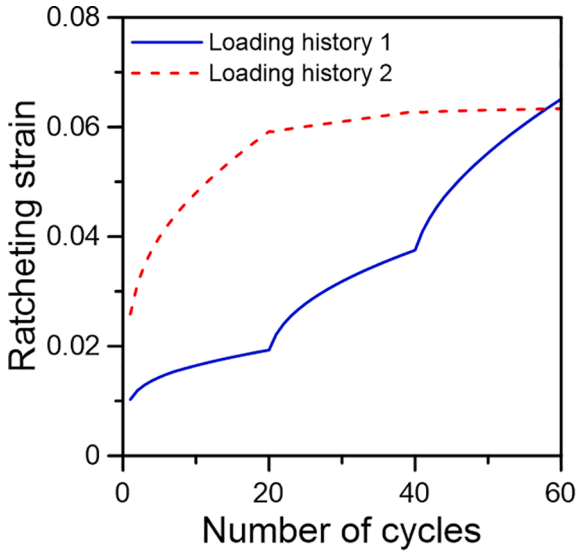

Fig. 13. Ratcheting strain with multi-step bending.

5.3. Compared with ratcheting boundary determined by two methods

To illustrate the two calculation criteria, the ratcheting boundary of oblique nozzles with local wall thinning was calculated by C-TDF and LMM methods respectively. Ratcheting boundary is expressed by the relationship between internal pressure and cyclic bending range, as shown in Fig. 17. Ratcheting boundary determined by the LMM is inconsistent with that of C-TDF. This phenomenon was found by Abdalla et al. [30] that used to simplify technical method. In order to verify the phenomenon, linear matching method is used to predict ratcheting boundary of lateral nozzle of cylinder with local wall thinning subjected to constant internal pressure and cyclic bending loading. It is found that ratcheting boundary determined by the LMM is in well agreement with that of the references. Further, the reliability of the LMM is verified. Therefore, ratcheting boundary of the lateral nozzle of cylinder with local wall thinning is determined by LMM in the following.

5.4. Ratcheting boundary of lateral nozzle of cylinder with local wall thinning

5.4.1. Effect of defect depth on ratcheting boundary

The ratcheting boundaries of the component with three defect depths of the lateral nozzle of cylinder, i.e., 1.05, 1.75 and 2.45 mm, are shown in Fig. 18. It can be indicated that the defect depth of the lateral nozzle of cylinder can significantly affect the reverse plasticity and ratchet limit. The increase of the defect depth can induce a remarkable increase of the reverse plasticity and the ratchet limits of the component.

5.4.2. Effect of defect length on ratcheting boundary

The ratcheting boundaries for three defect lengths, i.e., $h = 9.4$, 18.8 and 28.2 mm, are displayed in Fig. 19. It can be observed that the defect length has a slight effect on the reverse plasticity and ratchet limits of the component for all loading conditions mentioned. In addition, considering that the defect length does not manifest a remarkable difference on effective plastic strain distribution, so the corresponding strain distributions are not provided herein.

5.4.3. Effect of defect circumferential angle on ratcheting boundary

The ratcheting boundaries of the component with three defect circumferential angles of the lateral nozzle of cylinder, i.e., 30°, 60°and 90°, are given in Fig. 20. It can be indicated that the defect circumferential angle of the lateral nozzle of cylinder can significantly affect the reverse plasticity and ratchet limit. The increase of the defect circumferential angle can induce a remarkable increase of the reverse plasticity and the ratchet limits of the component.

6. Conclusions

In this study, the lateral nozzle of cylinder with local wall thinning is analyzed using Chaboche kinematic hardening rule by ANSYS. The conclusions drawn through numerical investigations are summarized as follows:

(1) The ratcheting strain of the lateral nozzle of cylinder with and without local wall thinning under cyclic bending loads is studied. It is found that the existence of local wall thinning would cause more obvious stress concentration phenomenon and ratcheting

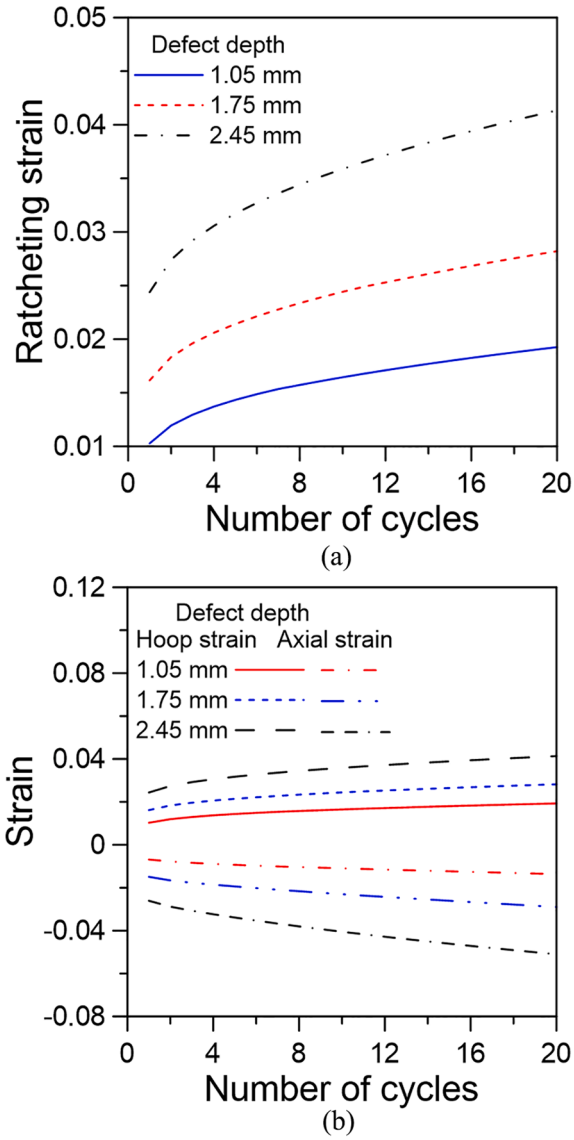

Fig. 14. Ratcheting strain of Point A.

Table 4
Numerical matrix for lateral nozzle of cylinder with local wall thinning.

No.	Defect depth d/mm	Defect length h/mm	Defect hoop angle θ/°	Notes
1	1.05	9.4	30	
2	1.75	9.4	30	Fixed h = 9.4 mm, θ=30°, change d's value.
3	2.45	9.4	30	
4	1.05	9.4	30	
5	1.05	18.8	30	Fixed d = 1.05 mm, θ=30°, change h's value.
6	1.05	28.2	30	
7	1.05	9.4	30	Fixed d = 1.05 mm, h = 9.4 mm, change θ's value.
8	1.05	9.4	60	
9	1.05	9.4	90	

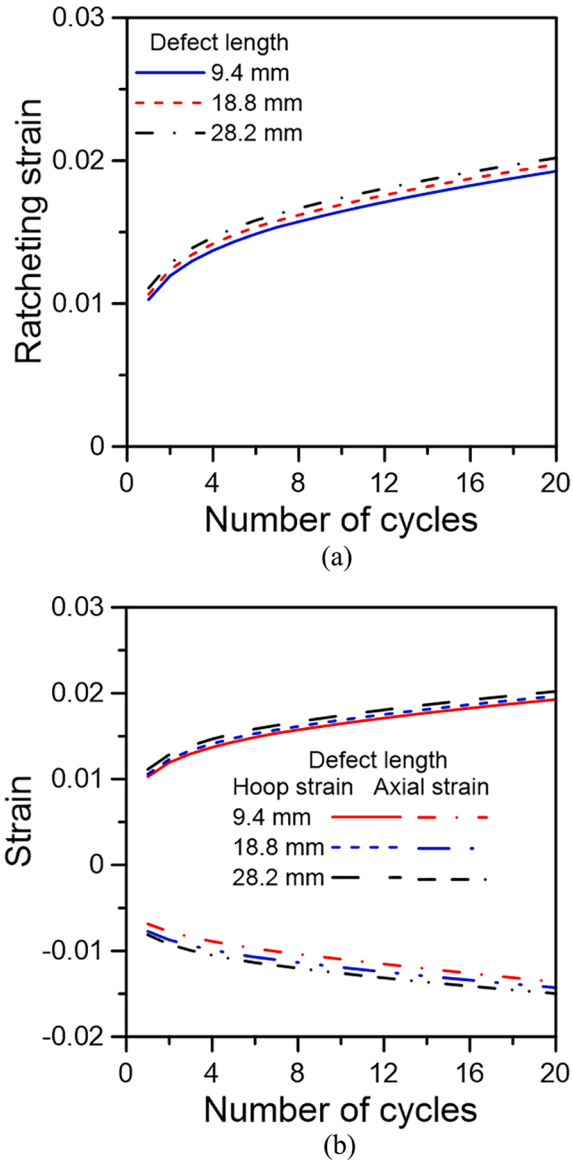

Fig. 15. The ratcheting strain prediction curve of the Point A of defective model.

effect for the location far from the defect, but the stress concentration phenomenon and ratcheting effect is relatively smaller. This study only concentrated on the sharp corner of the intersection region of the cylinder and nozzle. In order to help the experimental study of ratcheting strain of pipeline, the numerical values of axial plastic strain and hoop plastic strain of pipeline were also proposed to facilitate the experimental study and verification comparison. This study also found that the hoop plastic strain of the pipeline is obviously larger than the axial one.

(2) Aiming at the sharp corner part of the intersection region of the cylinder and nozzle, the influence of internal pressure, bending loading, loading paths and loading history on ratcheting strain of lateral nozzle of cylinder with local wall thinning is discussed. It is found that the ratcheting strain increases with the increase of internal pressure, and the ratcheting strain increases slowly. It indicates that the more the bending moment is, the more the ratcheting strain of pipeline is, and the ratcheting strain of pipeline increases slowly. Then, four different loading paths are applied on the lateral nozzle of cylinder with local wall thinning. It observes that the form of centralized force exerted on the pipeline has a significant impact on the ratcheting effect of the pipeline and different loading paths have a greater impact on the ratcheting effect of the pipeline. It investigates that the loading history of the pipeline has a great influence on the ratcheting effect of the pipeline.

(3) The influence of defect sizes on ratcheting effect of the lateral nozzle of cylinder with local wall thinning is also studied. It is found that the greater the defect depth, the greater the ratcheting strain of pipeline, and the slower the ratcheting strain of

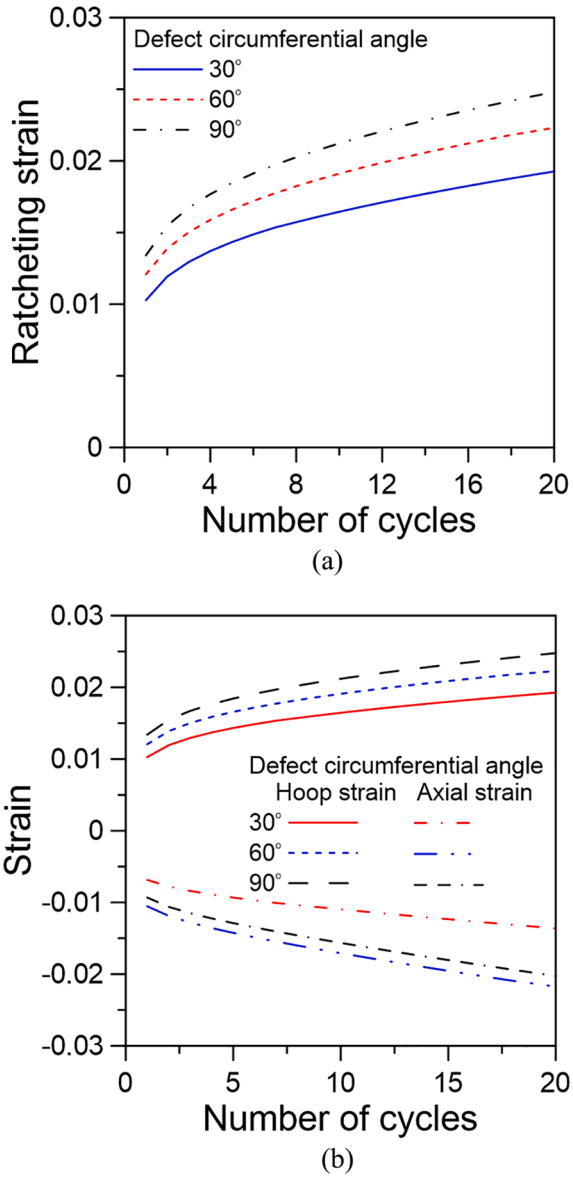

Fig. 16. The ratcheting strain prediction curve of the Point A of defective model.

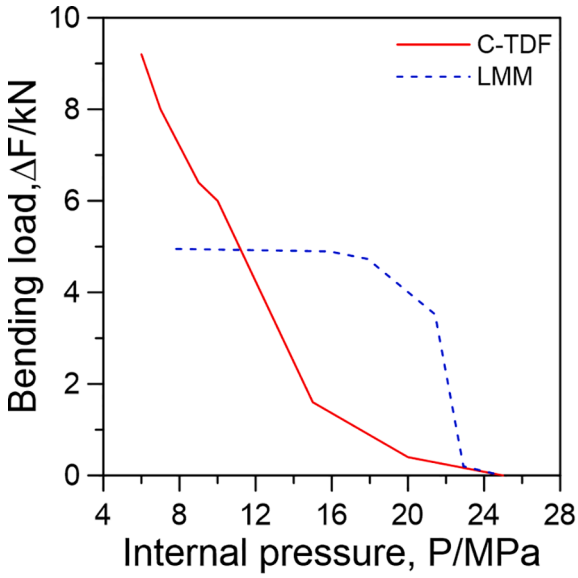

Fig. 17. Ratcheting boundary of lateral nozzle of cylinder with local wall thinning.

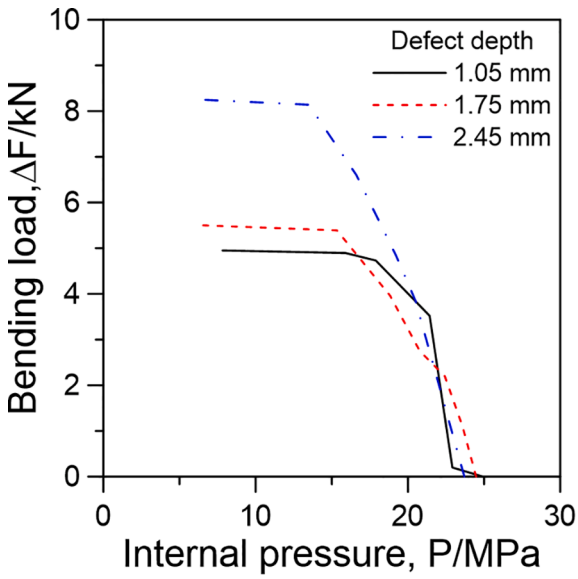

Fig. 18. Ratcheting boundary of lateral nozzle of cylinder with various defect depth.

pipeline increases; the larger the defect length, the ratcheting strain of pipeline has none change; the larger the defect circumferential angle, the ratcheting strain of pipeline first and then the smaller.

(4) For the stability of lateral nozzle of cylinder with local wall thinning, the ratcheting boundary curves of different defect sizes are calculated and studied. It found that the ratcheting boundary curve obtained by LMM standard is inconsistent with that of C-TDF standard. Based on LMM method, it found that the defect depth has obvious influence on the ratcheting boundary. The greater the defect depth, the greater the value of the ratcheting boundary; the defect length has no obvious influence on the ratcheting boundary of pipeline; the defect hoop angle has certain influence on the ratcheting boundary curve of pipeline, and the larger the defect circumferential angles, the greater the ratcheting boundary value.

Declaration of Competing Interest

The authors declare that they have no known competing financial interests or personal relationships that could have appeared to influence the work reported in this paper.

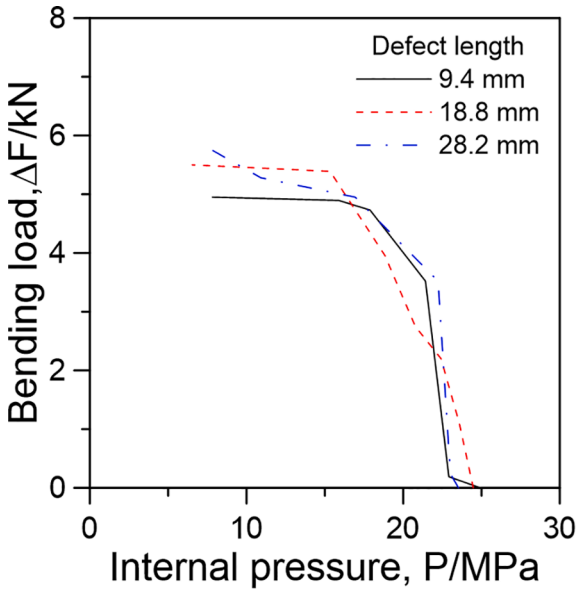

Fig. 19. Shakedown boundary of lateral nozzle of cylinder with various defect length.

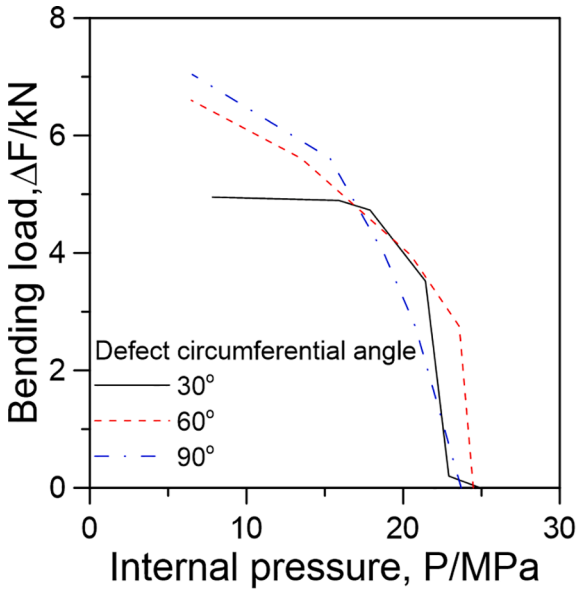

Fig. 20. Ratcheting boundary of lateral nozzle of cylinder with defect circumferential angle.

Acknowledgments

This work was partly supported by the Natural Science Foundation of Hebei Province of China (No. E2018501022), China Postdoctoral Science Foundation Funded Project (No. 2017M610171) and Fundamental Research Funds for the Central Universities (No. N182304009).

References

[1] A. Ravi Kiran, G.R. Reddy, M.K. Agrawal, Seismic fragility analysis of pressurized piping systems considering ratcheting: A case study, Int. J. Press. Vessels Pip. 169 (2015), pp. 031010-1–12.
[2] R. Karimi, M. Shariati, Experimental and numerical analysis of ratcheting behavior of ss 316 L thin-walled pipes subjected to cyclic internal pressure, J. Press. Vessels Technol. – Trans. ASME 142 (2020), pp. 061508-1–10.
[3] C.M. Liu, S.W. Shi, Y.B. Cai, X. Chen, Ratcheting behavior of pressurized-bending elbow pipe after thermal aging, Int. J. Press. Vessels Pip. 169 (2019) 160–169.

[4] M.A. Fenton, T. Hassan, Low-Cycle Fatigue Failure and Ratcheting Responses of Short and Long Radius Elbows at Room and High Temperatures, Master thesis, North Carolina State University, Raleigh, North Carolina, 2015.
[5] T. Hassan, M. Rahman, S. Bari, Low-cycle fatigue and ratcheting responses of elbow piping components, J. Press. Vessels Technol. – Trans. ASME 137 (2015).
[6] S.J. Zakavi, M. Zehsaz, R. EslamiM, The ratchetting behavior of pressurized plain pipework subjected to cyclicbending moment with the combined hardening model, Nucl. Eng. Des. 240 (2010) 726–737.
[7] S.J. Zakavi, M. Ajri, V. Golshan, The ratcheting behaviour of plain carbon steel pressurized piping elbows subjected to simulated seismic in-plane bending, World J. Mech. 4 (2014) 238–246.
[8] S.J. Zakavi, M. Nourbakhsh, The ratcheting behaviour of stainless steel pressurized piping elbows subjected to dynamic out-of-plane moments, Modern Mech. Eng. 4 (2014) 125–132.
[9] G.E. Varelis, S.A. Karamanos, A.M. Gresnigt, Pipe elbows under strong cyclic loading, J. Press. Vessels Technol. – Trans. ASME 135 (2013), pp. 011207-1–9.
[10] G.E. Varelis, S.A. Karamanos, Low-cycle fatigue of pressurized steel elbows under in-plane bending, J. Press. Vessels Technol. – Trans. ASME 137 (1) (2014), pp. 011401-1–10.
[11] X.H. Chen, X. Chen, D.J. Yu, B.J. Gao, Recent progresses in experimental investigation and finite element analysis of ratcheting in pressurized piping, Int. J. Press. Vessels Pip. 101 (2013) 113–142.
[12] X. Chen, B. Gao, G. Chen, Multiaxial ratcheting of pressurized elbows subjected to reversed in-plane bending, J. Press. Equip. Syst. 3 (2005) 38–44.
[13] X. Chen, B. Gao, G. Chen, Ratcheting study of pressurized elbows subjected to reversed in-plane bending, J. Press. Vessels Technol. – Trans. ASME 128 (2006) 525–532.
[14] H.R. Shi, G. Chen, Y. Wang, X. Chen, Ratcheting behavior of pressurized elbow pipe with local wall thinning, Int. J. Press. Vessels Pip. 102–103 (2013) 14–23.
[15] X.H. Chen, X. Chen, G. Chen, D.M. Li, Ratcheting behavior of pressurized Z2CND18.12N stainless steel pipe under different control modes, Steel Compos. Struct. 18 (2015) 29–50.
[16] X.H. Chen, X. Chen, W.W. Yu, D.M. Li, Ratcheting behavior of pressurized 90° elbow piping subjected to reversed in-plane bending with a combined hardening model, Int. J. Press. Vessels Pip. 137 (2016) 28–37.
[17] X.H. Chen, X. Chen, Effect of local wall thinning on ratcheting behavior of pressurized 90° elbow pipe under reversed bending using finite element analysis, Steel Compos. Struct. 20 (2016) 931–950.
[18] J. Shen, H.F. Chen, Y.H.A. Liu, New four-dimensional ratcheting boundary: Derivation and numerical validation, Eur. J. Mech. A-Solids 71 (2018) 101–112.
[19] R. Adibi-Asl, W. Reinhardt, Ratchet boundary determination using a noncyclic method, J. Press. Vessels Technol. – Trans. ASME 132 (2010) 021201.
[20] X.T. Zheng, H.Y. Peng, J.Y. Yu, W. Wang, W. Lin, J.M. Xu, Analytical ratchet limit for pressurized pipeline under cyclic nonproportional loadings, J. Pipeline Syst. Eng. Pract. 8 (3) (2017) 04017002.
[21] H.F. Chen, A.R.S. Ponter, A direct method on the evaluation of ratchet limit, J. Press. Vessels Technol. – Trans. ASME 132 (2010) 041202.
[22] L.D. Yang, J.H. Dong, B.J. Gao, X.P. Shi, Ratcheting study of pressurized lateral nozzle of cylinder of cylinder subjected to cyclic in-plane bending, Press. Vessels 27 (2010) 11–15 (in Chinese).
[23] X. Xia, Reliability of assessment of corroded subsea pipeline, Master thesis, Harbin Engineering University, Harbin, China, 2009.
[24] C.X.A. Liu, Finite element analysis for plastic limit load of welded piping branch junctions, Master thesis, Beijing University of Chemical Technology, Beijing, China, 2003.
[25] M.W. Lu, H. Xu, Discussion on some important problems of design by analysis, Press. Vessles 23 (2006) 15–19 (in Chinese).
[26] J.L. Chaboche, Time-independent constitutive theories for cyclic plasticity, Int. J. Plast. 2 (1986) 149–188.
[27] P. Armstrong, C. Frederick, A mathematical representation of the multiaxial bauchinger effect, CEGB Report No RD/BN 731, 1966.
[28] S. Asada, N. Yamashita, A. Okamoto, I. Nishiguchi, Verification of alternative criteria for shakedown evaluation using flat head vessel, ASME PVP 439 (2002) 17–23.
[29] Y. Yamamoto, N. Yamashita, M. Tanaka, Evaluation of thermal stress ratchet in plastic FEA, ASME PVP 439 (2002) 3–10.
[30] H.F. Abdalla, M.M. Megahed, M.Y.A. Younan, Comparison of pipe bend ratchetting/shakedown test results with the shakedown boundary determined via a simplified technique. Proceedings of the ASME 2009 Pressure Vessels and Piping Division Conference, July 26–30, Prague, Czech Republic, 2009.